Proposal for electron quantum spin Talbot effect

W. X. Tang,[1,*] D. M. Paganin,[1] and W. Wan[2]
[1]*School of Physics, Monash University, Victoria 3800, Australia*
[2]*Ernest Orlando Lawrence Berkeley National Laboratory, 1 Cyclotron Road, Mail Stop 80R0114, Berkeley, California 94720, USA*
(Received 6 April 2011; published 27 February 2012)

We propose a spin-polarized Talbot effect for an electron beam scattered from a grating of magnetic nanostructures. Existing periodic magnetic nanostructures can be used in conjunction with electron-beam illumination to create a spin-polarized replica of the transversely periodic exit surface beam a Talbot length away. Experiments have been proposed to verify the effect in a two-dimensional electron gas and an atomically flat surface by spin-polarized scanning probe microscopy. This effect provides a new route to modulate electron spin distributions in two-dimensional space.

DOI: 10.1103/PhysRevB.85.064418 PACS number(s): 75.76.+j, 03.75.−b, 72.25.−b, 75.70.Rf

I. INTRODUCTION

The ability to tune scalable semiconductor-based spintronics devices, based on the intrinsic spin of electrons to store and manipulate information, is both important and highly challenging for spin-based electronics since spin injection, spin accumulation, and spin modulation of electrons are required.[1–5] Currently, manipulation of the spin during transport between injector and detector via spin precession and spin pumping can be accomplished;[6] however, those methods have difficulty controlling spin distributions. By contrast, local tunability of spin distributions over nanometer scales is crucial for future solid-state quantum computers based on electron spin.[7] Inspired by the progress in fabricating and controlling nanoscale magnetic structures in low-dimensional systems, we propose a spin-dependent Talbot effect for electron waves scattered by a grating composed of magnetic nanostructures, to modulate the spin lattice pattern formed from a spin-polarized replica of the structure upon propagation through a Talbot length period and adjustable by controlling the electron wavelength and magnetic nanostructure period.

The optical Talbot effect was discovered in 1836[8] and later explained by Rayleigh as a natural consequence of Fresnel diffraction. He showed that the Talbot length $\mathcal{Z}_T$ is given by $\mathcal{Z}_T = 2a^2/\lambda$ (Ref. 9) in the paraxial approximation $a \gg \lambda$, where a is the period of the grating and λ is the wavelength of the incident light. However, in the nonparaxial regime where $\lambda \leqslant a < 2\lambda$ in Fig. 1, the Talbot effect is also operative for nonevanescent components of the scattered beam.[10] This effect reveals the wave nature of both radiation and matter wave fields, examples of the latter including atoms, electrons, and plasmons.[10–15]

Here, we demonstrate the existence of a spin-polarized nonparaxial Talbot effect for electron matter waves scattered by a grating composed of magnetic nanostructures. We find that the spin asymmetry of the scattered field varies with distance from the grating, creating an electron spin replica of the structure a Talbot length away, in a nonparaxial regime where $\lambda \leqslant a < 2\lambda$. This creates a tunable spin lattice in two-dimensional space, which is a powerful method to manipulate electron spin distributions in solid-state systems. We find that the spin interference pattern strongly depends on the wavelength and grating period; furthermore, the effect of a polyenergetic electron beam has been studied. Based on our theoretical results, we propose an experiment to verify this quantum spin Talbot effect (QSTE) in a two-dimensional electron gas (2DEG) system and an atomically flat surface by spin-polarized scanning probe microscopy. The potential applications in spintronics devices are proposed based on the QSTE.

II. THEORY

For a one-dimensional grating with period a, normally illuminated with a monoenergetic electron plane wave, the two-component spatial electron wave function $\{\psi_+, \psi_-\}^T$ at energy E and at any distance $z \geqslant 0$ downstream of the exit surface $z = 0$ is

$$\psi_\pm(x,z;E) = \sum_m c_m^\pm(E) \exp[i(\gamma_m x + t_m z)]. \qquad (1)$$

Here, x is the transverse coordinate, $c_m^\pm(E)$ denotes the Fourier coefficients of the two independent electron spin projections, $\gamma_m = 2\pi m/a$, and $t_m = \sqrt{(2\pi/\lambda)^2 - \gamma_m^2}$;[10,13,14] $\lambda = h/\sqrt{2m_e E}$ is the de Broglie wavelength, h is Planck's constant, and m_e is the electron mass. + and − represent "spin up" and "spin down" states of electron spin, respectively.

Consider a grating formed by nanoscale magnetic structures, for example, magnetic stripe domains, as shown in Fig. 2. Electron waves have a different complex transmission coefficient depending on the configuration of the incoming electron-beam spin state relative to the magnetization direction of magnetic domains [parallel ($\uparrow\uparrow$, $\downarrow\downarrow$) or antiparallel ($\uparrow\downarrow$, $\downarrow\uparrow$)].[1,2,5] Consequently, in an ideal situation, the spin up (down) electron wave ψ_+ (ψ_-) propagates through the up (down) magnetic domains in the grating, therefore achieving separation of the electron wave depending on the spin state, as shown in Fig. 2(a). The electron wave ψ_+ passes through the magnetic "up" domains A (green) with 100% transmission while being blocked completely by domains B (red). The color denotes the magnetization direction of a single domain. The corresponding probability density diffracted from the magnetic grating is longitudinally periodic in z with period equal to $\mathcal{Z}_T$. Simultaneously, the probability density depends on the spin of the electron wave shown in Fig. 2(a), as given by

$$\rho_\pm(x,z;E) = \sum_m \sum_n c_m^{\pm *}(E) c_n^\pm(E) H_{m,n}(x,z;E), \qquad (2)$$

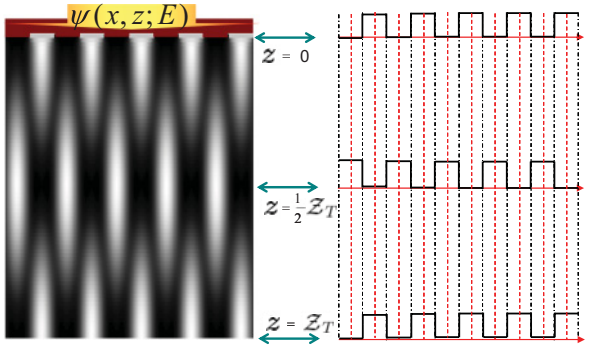

FIG. 1. (Color online) Principles of the nonparaxial Talbot effect, in which illumination of a grating with period a yields the first self-image at propagation distance $\mathcal{Z}_T = 75$ nm. Note that the paraxial formula gives $\mathcal{Z}_T = 2a^2/\lambda = 80$ nm. Here, $a = 20$ nm and $\lambda = 10$ nm.

where

$$H_{m,n}(x,z;E) = \exp\{i[(\gamma_n - \gamma_m)x + (t_n - t_m^*)z]\}. \quad (3)$$

By definition, the spin asymmetry

$$\aleph(x,z;E) \equiv \frac{\rho_+(x,z;E) - \rho_-(x,z;E)}{\rho_+(x,z;E) + \rho_-(x,z;E)} \quad (4)$$

will have the same longitudinal periodicity as the probability density. Since both the numerator and the denominator have a longitudinal periodicity, when either $a \gg \lambda$ or $\lambda \leqslant a < 2\lambda$, Eq. (4) implies a *continuously tunable spin lattice* in two-dimensional space as shown in Fig. 2(b). The distribution of two-dimensional spin asymmetry is determined by λ and a. In Fig. 2, $\lambda = 10$ nm and $a = 20$ nm; the numerically calculated Talbot distance $\mathcal{Z}_T$ is 75 nm instead of 80 nm as expected by the conventional formula $2a^2/\lambda$. The discrepancy is due to the paraxial approximation in conventional Talbot theory. To calculate the nonparaxial $\mathcal{Z}_T$ by the self-imaging condition $\rho_\pm(x,n\mathcal{Z}_T;E) = \rho_\pm(x,0;E)$, for integer n and $\lambda \leqslant a < 2\lambda$, we obtain[10]

$$\mathcal{Z}_T = \frac{\lambda}{1 - [1 - (\lambda/a)^2]^{1/2}}. \quad (5)$$

From Eq. (5), $\mathcal{Z}_T = 74.64$ nm, consistent with our numerical results based on Eqs. (2)–(4). In the paraxial limit where $a \gg \lambda$, Eq. (5) approaches $2a^2/\lambda$. This is consistent with the literature.[10,13,14] The spin asymmetry distribution [Fig. 2(b)] in the range $0.5 < \zeta \leqslant 1$, where $\zeta = \lambda/a$, is

$$\aleph(x,z;E) = A_0(x)\sin\frac{2\pi z}{\mathcal{Z}_T}, \quad (6)$$

where

$$A_0(x) = \frac{\sin\frac{2\pi x}{a}}{\frac{\pi}{8} + \frac{2}{\pi}\sin^2\frac{2\pi x}{a}}. \quad (7)$$

Note that evanescent waves have been neglected in calculating the above expression. If $x = a/4$, then $A_0 \approx 0.97$ as shown in Fig. 2(b). Because the spin Talbot distance $\mathcal{Z}_{T,S} = \mathcal{Z}_T$, spin lattices can be tailored through nm to sub-μm length scales depending on ζ and a.

To understand this tunability, we calculated the spin Talbot effect for different λ, with results shown in Fig. 3 for $\zeta = 0.1$,

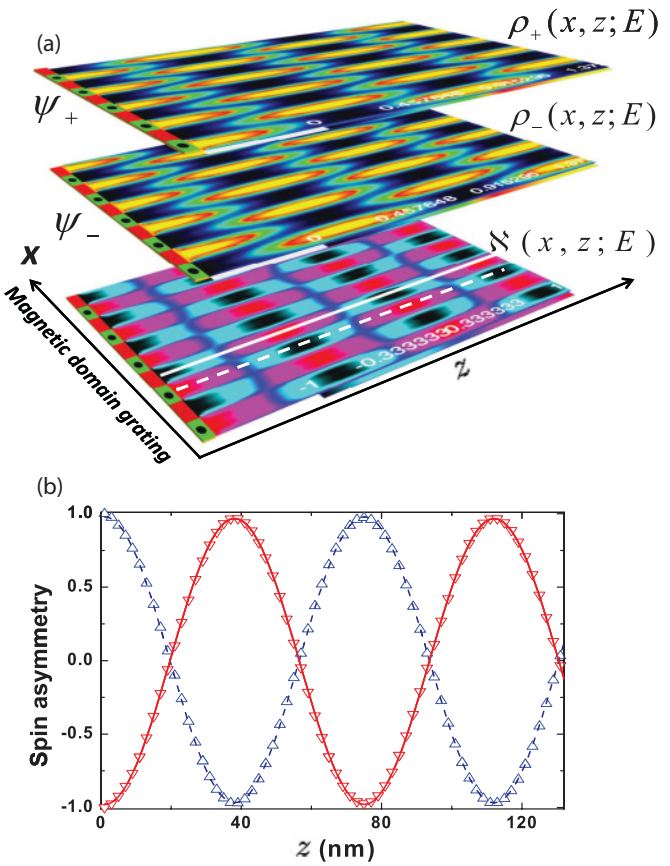

FIG. 2. (Color online) Normalized diffraction intensity and profiles. (a) Maps for spin up ρ_+ and down ρ_- probability density with spin asymmetry $\aleph(x,z;E)$. (b) Two spin asymmetry profiles along z are indicated by symbols $\triangle$ and $\triangledown$, and fitted by Eq. (6), where $a = 20$ nm, $\lambda = 10$ nm, and $\mathcal{Z}_T = 75$ nm from Eq. (5).

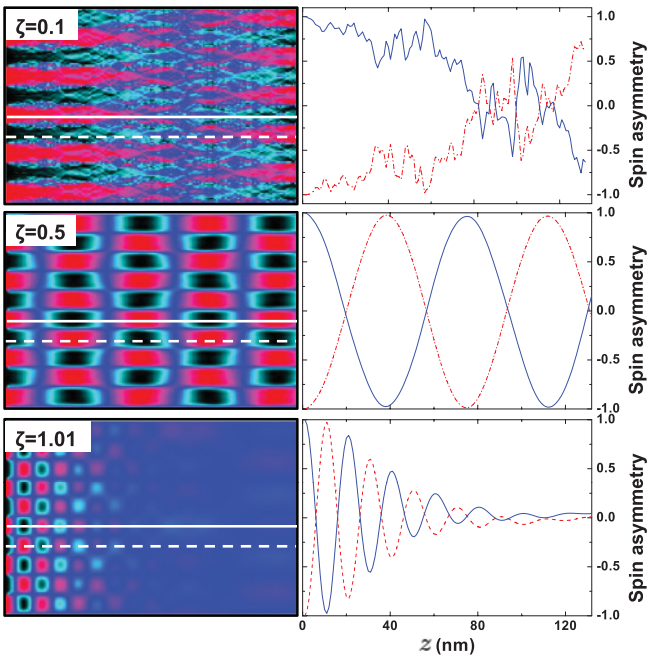

FIG. 3. (Color online) Two-dimensional spin distribution $\aleph(x,z;E)$ and corresponding profiles for $\zeta = 0.1$, 0.5, and 1.01, respectively.

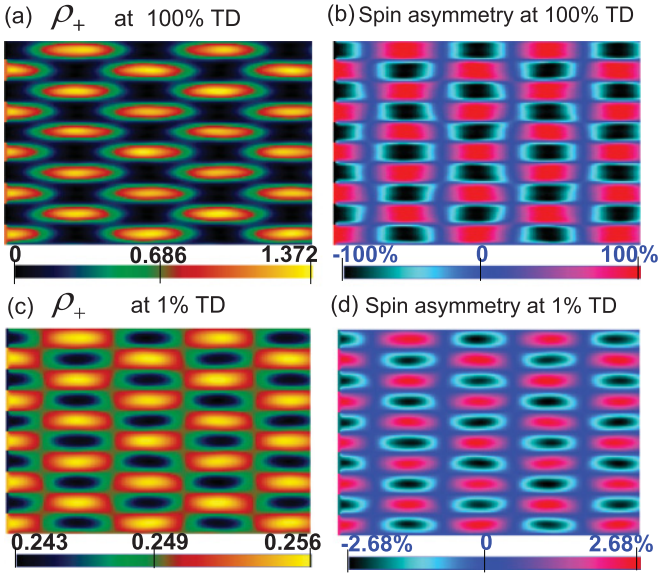

FIG. 4. (Color online) The spin asymmetry distribution dependent on transmission-rate difference between two channels. $a = 20$ nm and $\lambda = 10$ nm. (a), (b) are the plots of ρ_+ and $\aleph$ at 100% TD; (c), (d) are at 1% TD.

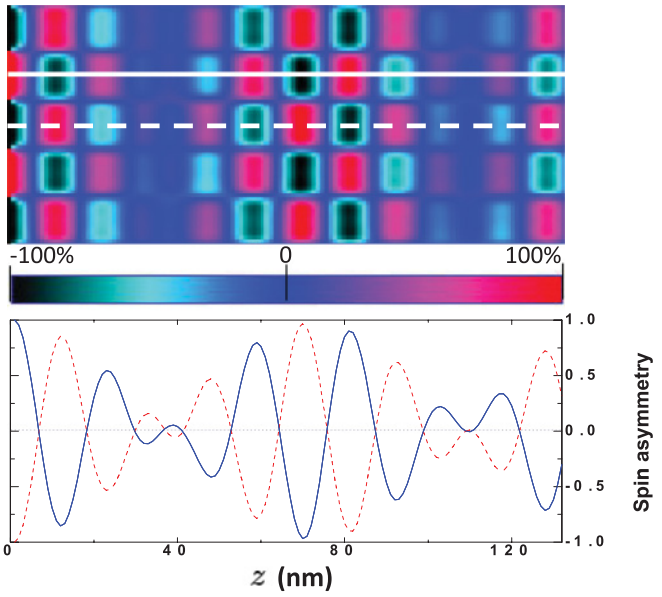

FIG. 5. (Color online) Polyenergetic spin asymmetry corresponding to $S_i(E) =$ constant in range $\lambda = 15$–20 nm, using 800 integral steps in the numerical integration; $a = 20$ nm.

0.5, and 1.01. We find that the spin asymmetry profile curves show a simple sine relationship when $0.5 < \zeta \leqslant 1$. However, if $\zeta < 0.5$, the curves have complex structures and small ripples decorate the spin asymmetry distribution (e.g., $\zeta = 0.1$); when $\zeta > 1$, evanescent waves imply that the polarization of spin decreases exponentially along z (e.g., $\zeta = 1.01$); Eqs. (5) and (6) are not applicable for these ranges. Movie 1 in the Supplemental Material shows sequential evolution of the $\rho_\pm$ and spin asymmetry $\aleph$ with ζ at $a = 20$ nm.[16]

In a more realistic model, the electron wave undergoes partial transmission at the antiparallel configuration between spin orientation and magnetization direction of the domain. Considering this, we find that the probability density distributions are blurred but nevertheless distinguishable; even assuming only 1% transmission difference (TD) between two channels, the intensity contrast and spin polarization drop with TD by the same order of magnitude (Fig. 4); however, the quantum spin Talbot effect is still observable.

The above discussions assume a monoenergetic electron wave. In a real system, to allow for a finite energy spread in the electron wave, assume an incident distribution of electron energies $S_i(E)$. Under this model, Eq. (4) generalizes to

$$\overline{\aleph}(x,z) \equiv \frac{\int S_i(E)\aleph(x,z;E)dE}{\int S_i(E)dE}. \tag{8}$$

The influence of energy spread on the 2D spin Talbot effect is calculated by numerical evaluation of $\overline{\aleph}(x,z)$, assuming $S_i(E)$ to be uniform from $\lambda = 15$ nm to 20 nm, with the results shown in Fig. 5. A dramatic longitudinal modulation of spin polarization near the grating is observed; consequently, the spin Talbot distance is also modulated depending on the energy spread $S_i(E)$. In Fig. 5, instead of one peak appearing within each spin Talbot distance, multiple peaks appear. The details of the spin asymmetry profile depend on $S_i(E)$ and need to be studied for real situations given known conditions. Therefore, to verify the quantum spin Talbot effect, a narrow energy spread is highly desired, or the method itself should have high energy resolution to distinguish different energy channels.

III. DISCUSSION

A 2DEG at interfaces such as in a GaAs/AlGaAs heterostructure is a candidate for testing the effect due to small energy spread at the Fermi level. In addition, the high mobility of electrons ($>3 \times 10^6$ cm^2 V^{-1} s^{-1}) and their long spin transportation distance (>100 μm) are suitable properties for spatial imaging of this effect.[5,19–23] The electron de Broglie wavelength at the Fermi energy is unusually long, around 20–100 nm,[21] making it possible to design a suitable magnetic domain period a and minimize effects caused by nonzero domain wall width.[17,18] Further concern includes suitable materials for the grating formed by magnetic stripe domains. The wavelength of electrons in metal is normally less than 1 nm; therefore, diluted magnetic semiconductors such as MnGaAs might be suitable to form magnetic domain gratings with similar band structure to AlGaAs/GaAs. Furthermore, by applying a pulsed spin-polarized electron current along the grating, the period a might be tunable by domain wall motion.[24,25] This capacity has been demonstrated elegantly in racetrack technology for 2D and 3D configuration by the Parkin group at IBM.[25] In their case, the $Fe_{18}Ni_{81}$ nanowire is applied and the writing speed can be around one nanosecond. It will be very interesting to have further study on the FM/2DEG interface properties, in particular, the magnetic properties of the magnetic nanowire on the surface of GaAs and the spin injection at the interface.[26,27]

We have described the properties of a 2DEG system for testing the effect; however, to carry out real measurements on the system, a spin-dependent spatial imaging method is needed. A spatial imaging technique has been elegantly applied

in spin Hall effect detection in a 2DEG system by scanning magneto-optic Kerr microscopy (SMOKE).[28] SMOKE is sensitive to spin polarization but with limited spatial resolution due to Abbe's law; it is ideal to demonstrate the principle of the spin-polarized effect on the micron scale.

Besides SMOKE, imaging electron flow in a 2DEG at the nanoscale has been achieved based on a scanning probe method.[22,29] But this can not be applied to verify the effect at GaAs/AlGaAs interfaces. However, scanning tunneling microscopy with a spin polarized tip (SP-STM) could be ideal for investigating the electron-spin-polarized Talbot effect on surfaces,[30–32] as it provides both spin contrast and atomic resolution. To our knowledge, we have yet to see the signature of the spin Talbot effect from the results of SP-STM. Recently, spin-dependent quantum interference within a Co magnetic nanostructure by SP-STM has been reported.[32] Inspired by this experiment, we believe SP-STM could be used to see the effect on an atomically flat surface;[33,34] electrons scattered by a grating formed by an antiferromagnetic atomic chain on an atomically flat surface could be an ideal system. Assuming $a = 0.65$ nm and $\lambda = 0.325$ nm, $\mathcal{Z}_T = 2.4$ nm from Eq. (5); therefore, a 300 nm atomically flat surface may provide an ideal platform to detect the effect, considering the space required to connect electrodes for applying current. One of the advantages of SP-STM is its energy resolution in dI/dV spin-asymmetry spectra to differentiate energy channels caused by nonzero energy spread.[32,33] A first-principles calculation needs to be carried out to consider the impact of surface band structures on the spin Talbot effect. This opens the possibility to create a long-distance spin correlation through Talbot self-imaging.[32]

Regarding applications of the QSTE in spintronics devices, a non-spin-polarized electron Talbot interferometer has been experimentally achieved in vacuum.[15] Given the spin Talbot pattern obtained, it is straightforward to form a quantum spin Talbot interferometer (QSTI) (Fig. 6). The QSTI will be sensitive to the magnetization orientation of magnetic quantum dots if they are located within the wave fronts of the incoming beam. This is useful to read out the spin state of quantum dots and spin correlations.

With electrodes connected at two gratings (G1 and G2) (Fig. 7), the quantum spin Talbot transistor (QSTT) device can be constructed. By calculating the spin transmission probability $T_{\pm}(\lambda, S)$ from Eq. (2) as an approximation, we

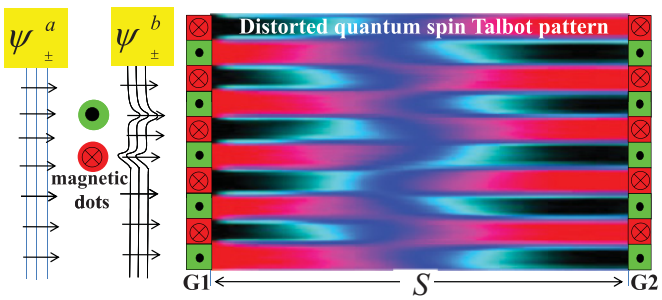

FIG. 6. (Color online) Schematic picture represents the deformation of spin Talbot pattern caused by the spin-dependent scattering at quantum-dot pairs in front of a grating.

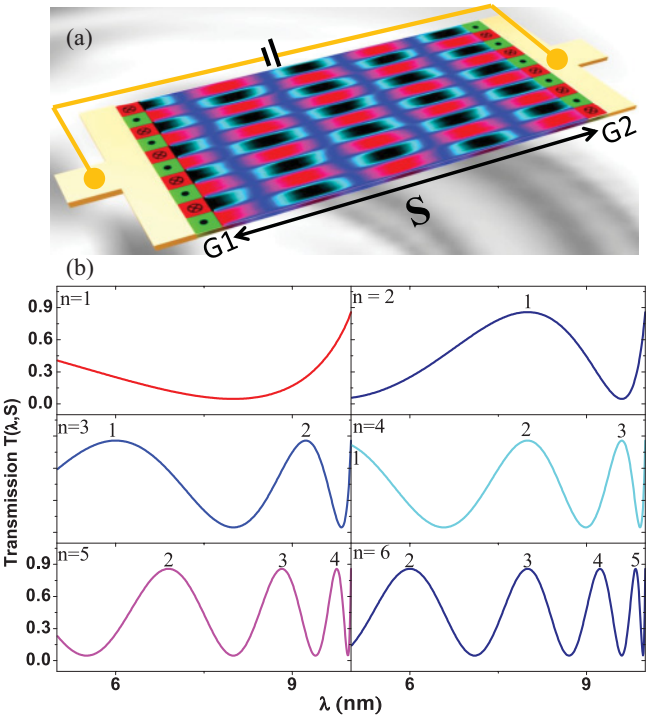

FIG. 7. (Color online) (a) Schematic picture of spin Talbot resistor device. (b) Characteristic spin Talbot resistance depends on grating distance and λ.

obtain

$$T(\lambda, S) = \frac{1}{4} + \frac{2}{\pi^2} + \frac{4}{\pi^2} \cos \frac{2\pi S}{\mathcal{Z}_T(\lambda)}, \tag{9}$$

where S is the distance between G1 and G2. The QSTT resistance curve is adjustable; it varies from single to multiple peaks depending on the ratio of S to λ. This formula is calculated by neglecting the electrical field applied in between the two gratings. By further considering the effect of an electric field, a modification in the previous equation will include an Airy function $\mathrm{Ai}(S)$.[35–37]

The nonspin electron Talbot effect has been verified by experiments in vacuum.[15] For the QSTE, one concern is the deflection due to the Lorentz force; however, it can be neglected due to ultrathin magnetic gratings (a few nm thick) and very low energy electrons. The deflection angle of an electron beam due to the Lorentz force is $\theta = eB\lambda t/h$, where e is the charge of electron, λ is the wavelength of electron, and t is the thickness of the magnetic grating. Assuming $t = 1$ nm, $\lambda = 10$ nm, and $B = 1$ T, θ is about 76 μm. This small deflection can be completely neglected at the nanometer scale and is much smaller than typical Bragg angles for electron diffraction, which are in the range of mrad. In the suggested systems, there is no applied magnetic field, and the spin lattice is caused by the spin-dependent distribution of electron density. The spin-flip processes such as Majorana flips are minor effects and have no direct impact on the QSTE effect.

It is necessary to distinguish the gratings which operate in the Raman-Nath or the Bragg regimes as thin and thick gratings, respectively.[38] Klein and Cook introduced a parameter Q, defined as $2\pi\lambda L/\Lambda^2 n_0$ (where L is the grating

thickness, λ is the wavelength of the electron, Λ is the grating spacing, and n_0 is the mean refractive index) to distinguish between the two regimes: If $Q < 1$, Raman-Nath operates; $Q > 10$ corresponds to the Bragg regime. In our case, given $L = 1$ nm, $\lambda = 100$ nm, and assuming $n_0 = 1$, $Q = 0.0628 < 1$. Therefore, the thickness of the grating should be thinner to avoid the Bragg regime.

Furthermore, the Talbot effect is a near-field effect. One interesting question will occur immediately, for the far-field situation: Can the QSTE survive? The answer is no. This far-field regime has been addressed for the nonspin electron Talbot effect in McMorran's work in vacuum.[15] According to their calculation, for the QSTE case, the smearing out of the spin asymmetry is expected. The second fact is the limited spin coherence distance in the 2DEG of around 10–100 μm which is also not favorable for the far field.

IV. CONCLUSION

In conclusion, we propose an electron-spin-polarized Talbot effect using electron waves scattered from a periodic magnetic nanostructure. We find that the spin asymmetry varies with distance from the grating, creating a spin-polarized replica of the structure a Talbot length away. This length is controllable by adjusting the electron wavelength λ and the grating period a. Experiments have been suggested to verify this effect. The success of the experiment will provide a new route to actualize periodic spin state distributions in two-dimensional space in solid devices. The quantum spin Talbot transistor and interferometer are suggested for future spintronics applications.

ACKNOWLEDGMENTS

We thank the referees for pertinent comments and suggestions. W.X.T. thanks Zheng Gai at ORNL and Chun-Lei Gao at SJTU for illuminating discussions on potential experimental verification. W.X.T. thanks S. A. Crooker and Hanan Dery for helpful discussion.

*wenxin.tang@monash.edu

[1] P. Grunberg, R. Schreiber, Y. Pang, M. B. Brodsky, and H. Sowers, Phys. Rev. Lett. **57**, 2442 (1986).
[2] M. N. Baibich, J. M. Broto, A. Fert, F. Nguyen Van Dau, F. Petroff, P. Etienne, G. Creuzet, A. Friederich, and J. Chazelas, Phys. Rev. Lett. **61**, 2472 (1988).
[3] G. A. Prinz, Phys. Today **48**(4), 58 (1995).
[4] G. A. Prinz, Science **282**, 1660 (1998).
[5] S. A. Wolf, D. D. Awschalom, R. A. Buhrman, J. M. Daughton, S. von Molnar, M. L. Roukes, A. Y. Chtchelkanova, and D. M. Tregar, Science **294**, 1488 (2001).
[6] S. K. Watson, R. M. Potok, C. M. Marcus, and V. Umansky, Phys. Rev. Lett. **91**, 258301 (2003).
[7] A. Morello *et al.*, Nature (London) **467**, 687 (2010).
[8] H. F. Talbot, Philos. Mag. **9**, 401 (1836).
[9] Lord Rayleigh, Philos. Mag. **11**, 196 (1881).
[10] E. Noponen and J. Turunen, Opt. Commun. **98**, 132 (1993).
[11] M. S. Chapman, C. R. Ekstrom, T. D. Hammond, J. Schmiedmayer, B. E. Tannian, S. Wehinger, and D. E. Pritchard, Phys. Rev. A **51**, 14R (1995).
[12] A. D. Cronin and B. McMorran, Phys. Rev. A **74**, 061602(R) (2006).
[13] M. R. Dennis, N. I. Zheludev, and F. J. G. Abajo, Opt. Express **15**, 9692 (2007).
[14] A. A. Maradudin and T. A. Leskova, New J. Phys. **11**, 033004 (2009).
[15] B. J. McMorran and A. D. Cronin, New J. Phys. **11**, 033021 (2009).
[16] See Supplemental Material at http://link.aps.org/supplemental/10.1103/PhysRevB.85.064418 for movie 1, which shows the change of two-dimensional $\rho_{\pm}$ and $\aleph$ distributions with ζ.
[17] N. Rougemaille and A. K. Schmid, Eur. Phys. J. Appl. Phys. **50**, 20101 (2010).
[18] Domain wall width w is determined by exchange interaction J and anisotropy K, and can be estimated from $w \propto \sqrt{J/K}$; w ranges from a few nm to μm.
[19] M. C. Holland, A. H. Kean, and C. R. Stanley, J. Cryst. Growth **127**, 793 (1993).
[20] D. D. Awschalom, Physica E **10**, 1 (2001).
[21] T. Chakraborty and P. Pietilainen, editors, *The Quantum Hall Effects: Integral and Fractional*, 2nd ed. (Springer-Verlag, New York, 1995).
[22] M. A. Topinka, R. M. Westervelt, and E. J. Heller, Phys. Today **56**(12), 47 (2003).
[23] A. Dourlat, C. Gourdon, V. Jeudy, K. Khazen, H. J. voon Bardeleben, L. Thevenard, and A. Lemaitre, Physica E **40**, 1848 (2008).
[24] A. Yamaguchi, T. Ono, S. Nasu, K. Miyake, K. Mibu, and T. Shinjo, Phys. Rev. Lett. **92**, 077205 (2004).
[25] L. Thomas, M. Hayashi, X. Jiang, R. Moriya, Ch. Rettner, and S. S. P. Parkin, Nature (London) **443**, 197 (2006).
[26] Private communication with Stuart Parkin and S. A. Crooker, respectively.
[27] S. A. Crooker, M. Furis, X. Lou, C. Adelmann, D. L. Smith, D. L. Palmstrom, and P. A. Crowell, Science **309**, 2191 (2005).
[28] V. Sih, R. C. Myers, Y. K. Kato, W. H. Lau, A. C. Gossards, and D. D. Awschalom, Nature Phys. **1**, 31 (2005).
[29] M. A. Topinka, B. J. LeRoy, S. E. J. Shaw, E. J. Heller, R. M. Westervelt, K. D. Maranowski, and A. C. Gossard, Science **289**, 2323 (2000).
[30] G. Binnig, H. Rohrer, Ch. Gerber, and E. Weibel, Appl. Phys. Lett. **40**, 178 (1982).
[31] R. Wiesendanger, H.-J. Guntherodt, G. Guntherodt, R. J. Gambino, and R. Ruf, Phys. Rev. Lett. **65**, 247 (1990).
[32] H. Oka, P. A. Ignatiev, S. Wedekind, G. Rodary, L. Niebergall, V. S. Stepanyuk, D. Sander, and J. Kirschner, Science **327**, 843 (2010).
[33] C . L. Gao, A. Ernst, A. Winkelmann, J. Henk, W. Wulfhekel, P. Bruno, and J. Kirschner, Phys. Rev. Lett. **100**, 237203 (2008).
[34] C. L. Gao, W. Wulfhekel, and J. Kirschner, Phys. Rev. Lett. **101**, 267205 (2008).
[35] D. M. Paganin and W. X. Tang (unpublished).
[36] S. M. Kennedy, D. M. Paganin, and D. E. Jesson, Am. J. Phys. **76**, 158 (2007).
[37] W. R. Klein and B. D. Cook, IEEE Trans. Sonics Ultrason. **SU-14**, 123 (1967).
[38] M. G. Moharam and L. Young, Appl. Opt. **17**, 1757 (1978).